The impact of surface heterogeneity on the diurnal cycle of deep convection

Received: 28 April 2021 | Revised: 21 July 2022 | Accepted: 23 August 2022 | Published on: 14 October 2022

DOI: 10.1002/qj.4371

Quarterly Journal of the Royal Meteorological Society RMetS

RESEARCH ARTICLE

The impact of surface heterogeneity on the diurnal cycle of deep convection

Natalie J. Harvey[1] | **Chimene L. Daleu**[1] | **Rachel A. Stratton**[2] | **Robert S. Plant**[1] | **Steven J. Woolnough**[3] | **Alison J. Stirling**[2]

[1]Department of Meteorology, University of Reading, Reading, UK

[2]Met Office, Exeter, UK

[3]National Centre for Atmospheric Science, University of Reading, Reading, UK

Correspondence
N. J. Harvey, Department of Meteorology, University of Reading, Reading, RG6 6ET, UK.
Email: n.j.harvey@reading.ac.uk

Funding information
Natural Environment Research Council, Grant/Award Numbers: R8/H12/83/001, NE/M017222/1, NE/N013743/1

Abstract

Despite some recent improvements, major deficiencies remain in model simulations using parameterised convection in capturing both the phase and amplitude of the daily cycle of precipitation in tropical regions. The difficulties are particularly acute in regions of heterogeneous surface conditions, since the simulations need not only to respond appropriately to the local forcing from surface fluxes but also to capture the interactions with near-surface mesoscale circulations. Here, we examine such a situation by means of idealised cloud-resolving simulations of deep convection over a heterogeneous surface, performed using the cloud-resolving simulation known as the Met Office NERC Cloud model (MONC). In these simulations, we show that precipitation forms preferentially over dry and warm patches ("DRY") compared with wet and cold patches ("WET"), with the peak precipitation rates differing by a factor of approximately 4. The initiation of precipitation occurs approximately 1.5 hr earlier in the DRY patches compared with the WET patches. Moreover, within the WET and DRY patches there are marked differences in the spatial distribution of the precipitation. These cloud-resolving simulations are then used as a benchmark to assess the behaviour of simulations using parameterised convection, performed using the idealised configuration of the Met Office Unified Model (MetUM). The MetUM simulations produce a response with some qualitative similarities to the cloud-resolving simulations. In particular, although the simulations with parameterised convection initiate precipitation too early, they are capable of capturing the relative amounts of daily-mean precipitation in the DRY and WET patches. We propose that the cloud-resolving simulations could be used further to investigate the impact of fully interactive surface schemes and as benchmark simulations to evaluate new parameterisation schemes.

KEYWORDS

cloud-resolving models, convective parameterisation, land–atmosphere interaction, rainfall

1 | INTRODUCTION

Simulating the diurnal cycle of deep convection is a long-standing problem in both numerical weather prediction (NWP) and climate modelling. There are major deficiencies in capturing both the phase and amplitude of the daily cycle of precipitation in tropical regions (e.g., Yang and Slingo, 2001; Lee *et al.,* 2008; Hohenegger and Stevens, 2013; Christopoulos and Schneider, 2021). This has implications on short weather time-scales for predicting flash floods and droughts (e.g., Dipankar *et al.,* 2020), and also limits the ability to plan for food and water security in our changing climate (e.g., Birch *et al.,* 2014).

In observations for tropical regions over land, precipitation intensity tends to peak in the late afternoon or early evening (Yang and Slingo, 2001; Liu and Zipser, 2008; Tan *et al.,* 2019). However, in NWP and global climate models (GCMs), the peak precipitation often occurs too early, alongside the peak in surface heating (e.g., Bechtold *et al.,* 2004; Dai, 2006; Stephens *et al.,* 2010; Nikulin *et al.,* 2012). The timing can be improved if the horizontal grid spacing is reduced enough to allow the development of explicit convection within the model (e.g., Clark *et al.,* 2007; Sato *et al.,* 2009; Pearson *et al.,* 2014), but this provides only a partial remedy and comes with a huge computational cost. Convective parameterisation in global models will still be needed for some time.

Improvements to the timing of the diurnal cycle of convection in parameterised models have been made by various methods. Some studies have embedded a cloud-resolving model within a lower resolution GCM (e.g., Khairoutdinov *et al.,* 2005; Dirmeyer *et al.,* 2012; Kooperman *et al.,* 2016), while another approach allows the entrainment rate over land to vary with the height of the lifting condensation level (Stratton and Stirling, 2012; Stirling and Petch, 2004). Bechtold *et al.* (2014) achieved improvements by modifying a Convective Available Potential energy (CAPE) closure scheme in order to distinguish between boundary-layer and free-tropospheric forcings, while Xie *et al.* (2019) did so by revising the triggering formulation to take account of dynamic as well as thermodynamic factors.

Another line of development has been based on the idea of adding one or more prognostic variables to carry information or "memory" of the previous behaviour of the unresolved processes. Colin *et al.* (2019) note that there is no consensus about which variable or variables should be considered as prognostic, as evidenced by a wide range of example studies (see references therein). Some additional approaches include the prognostic treatment of convective vertical velocity and area fraction by Gerard and Geleyn (2005), considerations of area fractions for multiple cloud types (Cardoso-Bihlo *et al.,* 2019), and a machine-learning-based approach for prognostic cloud-base mass flux (Hagos *et al.,* 2020).

Recent idealized cloud-resolving modelling studies by Colin *et al.* (2019) and Daleu *et al.* (2020) have demonstrated that memory from previous convective activity is retained by low-level thermodynamic structures on scales of $\mathcal{O}(10)$ km. Those authors did not show the origin for such structures, but pointed out that they might be produced as remnants of decaying cold pools, for example. Their results are consistent with Davies *et al.* (2009), who explored the persistence of similar structures on subdiurnal time-scales, and with Stirling and Petch (2004), who showed that, in a 2D setup, the diurnal cycle of unorganised convection is strongly affected by variability of relative humidity in the boundary layer.

The above modelling studies were based on time-varying but horizontally homogeneous scenarios, so that (aside from initial random perturbations) all spatial variability arose as a consequence of prior convective motions. In reality, spatial variability may also be induced by variations in surface conditions. Many observational studies in recent years have highlighted the importance of surface heterogeneity for the triggering and development of convection (e.g., Taylor *et al.,* 2011; Petrova *et al.,* 2018; Fast *et al.,* 2019). Differential heating patterns at the surface generate horizontal pressure gradients, which induce horizontal flows from cool/wet to warm/dry surfaces. Such flows are analogous to sea breezes (Segal and Arritt, 1992). Over land, the onset of these circulations can be due to the presence of gradients in soil moisture (Taylor *et al.,* 2007; Kang *et al.,* 2007), cloud shading (Marsham *et al.,* 2007b; Marsham *et al.,* 2007a), vegetation type and pattern (Garcia-Carreras *et al.,* 2010), and surface albedo (Marsham *et al.,* 2008).

Various modelling studies have focussed on the impacts of surface heterogeneity on boundary-layer circulations and the shallow cumulus clouds that are embedded within such flows (e.g., Patton *et al.,* 2005; Avissar and Schmidt, 1998; Kirshbaum and Fairman, 2015). Rieck *et al.* (2014) and Baur *et al.* (2018), however, studied the impact of heterogeneity on the development of deep convection in the midlatitudes. Lee *et al.* (2019) considered the transition from shallow to deep convection for a composite case study over the US Southern Great Plains, while Rochetin *et al.* (2017) considered the impact of a circular sensible heat flux anomaly on the transition to deep convection over a semi-arid region in the Sahel. A study by Cioni and Hohenegger (2018) provides an interesting perspective on the roles of local and advected moisture sources in determining the total precipitation within dry and moist patches.

The examples above show that there are good observational and modelling studies available for understanding

the influence of heterogeneity on scales of approximately 10–25 km. Also, many such studies advocate for (or are at least partially motivated by) incorporating such influences within parameterisations. However, this goal remains challenging, not least because of the multiple parameterisations involved in simulating the diurnal cycle of convection in a GCM or global-scale NWP model. Boundary-layer turbulence, shallow convection, and deep convection parameterisations are key at different stages within the diurnal cycle and a successful simulation requires that they interact with each other appropriately, as well as being able to respond appropriately to the heterogeneous conditions. Their interactions with parameterised radiation and microphysics can also have leading-order roles to play.

The goal of this article is to assess an idealized configuration that may provide a useful intermediate point to support model development, by isolating the role of the deep convection parameterisation. We consider the diurnal cycle in a configuration with prescribed surface fluxes and radiative cooling and without a distinct shallow phase, in which the first moist convective elements rise to the tropopause. The value of such idealisations and simplifications is that the configuration places the emphasis firmly on the response of the deep convection parameterisation to the surface heterogeneity and to the low-level circulations that may have developed as a result. This allows us to make a clean assessment of the performance of an example parameterisation, and so to isolate and highlight any deficiences in its response.

More specifically, we compare the simulations performed using a high-resolution cloud-resolving model against equivalent simulations using parameterised convection. The high-resolution simulations were performed using the new Met Office Natural Environment Research Council (NERC) Cloud model (MONC) and the simulations using parameterised convection were performed using the idealised version of the UK Met Office Unified Model (MetUM). The surface is formed from a patchwork of warm/dry and cool/wet areas, and various patch sizes and MetUM grid spacings are considered. Their relative sizes vary such that patches may be well resolved or may be at the grid scale in the case of the parameterised model. This allows for comparison of the response of the cloud-resolving model with a developing, resolved low-level circulation between the patches, as against a purely localised response from the parameterised model. Our analysis includes consideration of the timing of precipitation, its relative magnitudes for the patches, and its spatial distribution within the patches.

Section 2 describes the model setups and experimental design, with analysis of MONC and the idealised MetUM results being shown in Sections 3 and 4, respectively. A summary, conclusions, and implications for future work are presented in Section 5.

2 | MODEL DESCRIPTION AND EXPERIMENTAL DESIGN

2.1 | Met Office NERC Cloud Model—MONC

MONC (Brown *et al.,* 2015) is used in this study. MONC is a recent rewrite of the UK Met Office Large Eddy Model (LEM) to improve computational efficiency. The LEM has been used for numerous cloud and turbulence studies in a wide range of regimes for over two decades (e.g., Brown, 1999; Brown *et al.,* 2002; Marsham *et al.,* 2006; Davies *et al.,* 2009; Young *et al.,* 2017). Full details of the LEM can be found in Shutts and Gray (1994). MONC benefits from much-improved parallelisation and has been optimised such that simulations with large 3D domains can be run at high resolution. It has already been used to perform a number of studies on cloud microphysics (Dearden *et al.,* 2018), boundary-layer turbulence (Kealy *et al.,* 2019), equilibrium shallow and deep convection (Gu *et al.,* 2020), and the diurnal cycle of deep convection (Daleu *et al.,* 2020).

MONC solves a set of anelastic, quasi-Boussinesq equations. Lateral boundary conditions are biperiodic and the model top is buffered with a damping layer to absorb vertically propagating waves. Subgrid processes are parameterised using the Smagorinsky–Lilly approach. Cloud processes are represented using the Cloud AeroSol Interacting Microphysics scheme (CASIM), a configurable, multimoment bulk microphysics scheme that represents cloud water, rain, ice, snow, and graupel. CASIM has been developed to replace the microphysics scheme in the MetUM and has been used in a variety of studies (e.g., Shipway and Hill, 2012; Hill *et al.,* 2015; Grosvenor *et al.,* 2017; McCoy *et al.,* 2018; Miltenberger *et al.,* 2018). Note that this is a change from the microphysics scheme used in the LEM.

2.2 | The idealised Met Office Unified Model

To investigate the influence of surface heterogeneity on the diurnal cycle of deep convection with parameterised convection, a number of companion simulations were performed using the idealised configuration of the MetUM. The idealised MetUM can be configured to use the same dynamical core and parameterisation schemes as

the operational Met Office models, but uses a Cartesian rather than a latitude–longitude grid. It is assumed to be at a fixed latitude (f-plane) as far as the Coriolis term is concerned and has bicyclic boundary conditions. It can be initialised with simple profiles and forced by prescribed large-scale tendencies and surface fluxes in a similar way to MONC. It has been used to investigate a variety of atmospheric processes and phenomena (e.g., Boutle *et al.,* 2015; Volonté *et al.,* 2020; Wing *et al.,* 2020).

For this study the idealised MetUM is configured to run over a flat surface, located at the Equator, with roughness lengths appropriate for land as in the MONC simulations. The model radiation scheme is switched off. The model is run for several relatively coarse horizontal resolutions. It has a model top at 38.5 km and uses the bottom 63 levels of the standard vertical level set that is used for the operational global model (which has a top at 80 km). The vertical resolution is slighter higher than MONC for the lowest levels, but is coarser higher up (cf. Section 2.3.1). The MetUM uses a Charney–Phillips grid in the vertical, with the lowest potential temperature level being at 20 m and the lowest wind level at 10 m. The Even Newer Dynamics for General atmospheric modelling of the environment (ENDGame) dynamical core solves for a nonhydrostatic fully compressible deep atmosphere and is semi-implicit and semi-Lagrangian (Wood *et al.,* 2014). Although it does not exactly conserve energy, dry mass, and water locally, in this configuration it conserves dry mass and water for the bicyclic domain. Like MONC, the idealised MetUM uses a damping layer over the top quarter of the vertical domain in order to absorb vertically propagating waves. (This differs from the global MetUM, which has no damping but some diffusion and filtering *depending* on latitude.)

The idealised MetUM has been set up to use the suite of parameterisation schemes in the global atmospheric configuration known as GA7 (Walters *et al.,* 2019). A brief description of the parameterisations that are key for this diurnal convective case is given here. The boundary-layer scheme (Lock *et al.*, 2000) is a first-order turbulence closure scheme mixing momentum and conserved heat and moisture variables. The scheme applies mixing over the whole depth of the atmosphere. GA7 uses a mass flux convection scheme based on Gregory and Rowntree (1990), with many subsequent extensions, including convective momemtum transport and downdraughts. The convective parameterisation takes its diagnosis of whether convection is possible from the boundary-layer scheme (Lock *et al.,* 2000) and, if so, whether it will be shallow or deep. The shallow scheme includes different entrainment rates from the deep convection scheme and is more appropriate for shallow oceanic convection rather than nonequilibrium developing convection over land. Midlevel convection (convection triggering from above the boundary-layer top) is also possible. Over land, this may occur in the evening, when the near-surface boundary layer becomes stable such that deep convection can no longer be diagnosed. The GA7 convective parameterisation does not include the most recent extension to the convection scheme (Willett and Whitall, 2017), which links entrainment to the past history of precipitation, helping to improve the diurnal cycle of convection over land, and so suffers from the well-known problem of diurnal convection over land triggering too early in the day. The convection scheme is able to detrain condensate to the cloud scheme known as Prognostic Cloud Fraction and Prognostic Condensate (PC2: Wilson *et al.,* 2008). The large-scale microphysics scheme is that of Wilson and Ballard (1999) and this will operate on any large-scale anvil cloud detrained by the convection scheme.

2.3 | Experimental setup

2.3.1 | High-resolution simulations

MONC is employed to simulate an idealised diurnal cycle of deep convection over a flat tropical continental area. The computational domain spans $512 \times 512 \times 99$ grid points with a horizontal grid spacing of 200 m. In the vertical, a stretched grid ranges from a spacing of $\Delta z = 25$ m in the boundary layer up to $\Delta z = 500$ m in the free troposphere. As in earlier studies by Davies *et al.* (2009); Daleu *et al.* (2020), and as discussed in Section 1, the forcings for the case are designed such that deep convection develops as soon as moist convection occurs. In most other respects, the configuration follows that of the EUROpean Cloud Systems (EUROCS) case study over the southern Great Plains (Guichard *et al.,* 2004), including the initial temperature and humidity profiles as presented in Figure 1.

The lower boundary condition is set by specifying surface sensible and latent heat fluxes. In the homogeneous control simulation (M-CON) used for comparison in this study, these vary sinusoidally for the first 12 hr of the simulation, with peak values at t=6 hr, and between 12 and 24 hr the surface fluxes are set to zero. The peak values of the sensible and latent heat fluxes, 130 and 400 $\mathrm{W \cdot m^{-2}}$ respectively, are taken from observations of the EUROCS field campaign (Guichard *et al.,* 2004). With the exception of M-CON, we perform the high-resolution simulations for two days, taking the first as spin-up and analysing results from the second day. The M-CON simulation is extended to 10 days. This allowed us to check that the spin-up period

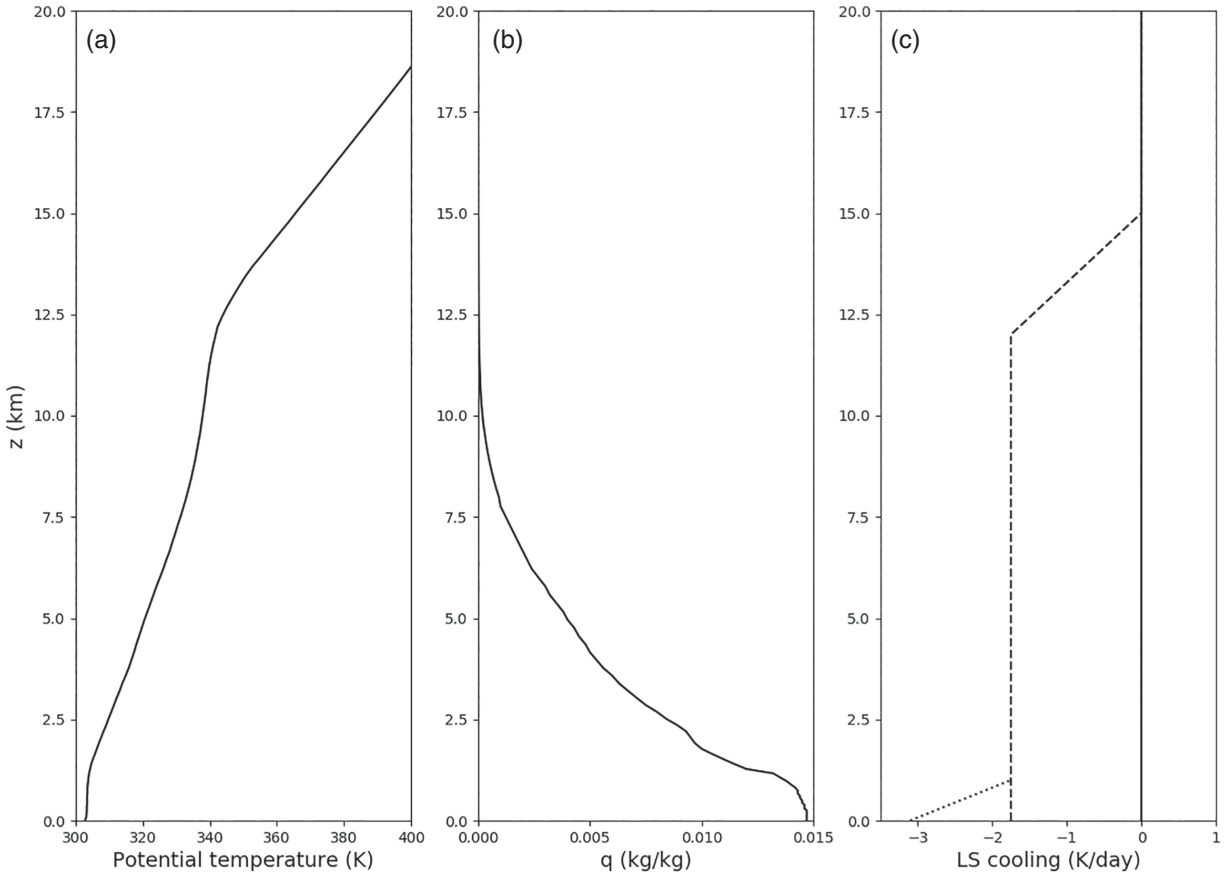

FIGURE 1 Profiles of (a) initial potential temperature, (b) initial specific humidity, and (c) the large-scale cooling profiles applied. In (c), the dashed and dotted lines show the daytime and night-time profiles, respectively

was sufficient and to provide an indication of the statistical variability in our results, based on the range for days 2–10. As in Daleu *et al.* (2020), a large-scale cooling profile is also applied, as shown in Figure 1c. Specifically, the cooling is $\partial\theta/\partial t = -1.75\,\mathrm{K{\cdot}d^{-1}}$ throughout the troposphere during the day, and an additional near-surface cooling of up to $-3.1\,\mathrm{K{\cdot}d^{-1}}$ is imposed at night. The cooling rates are chosen such that the column-integrated moist static energy budget is balanced by the combination of all forcings over the course of a day. The Coriolis force is set to zero and no mean wind is applied.

A variety of methods have been considered for introducing surface heterogeneity into numerical experiements, including simple stripes, patches, and checkerboard patterns in surface fluxes (Patton *et al.*, 2005; Courault *et al.*, 2007; Rieck *et al.*, 2014; Rochetin *et al.*, 2017b; Lee *et al.*, 2019), assignments based on land-use classes (Huang and Margulis, 2009; Maronga and Raasch, 2013) or surface precipitation patterns (Wu *et al.*, 2015), through to the use of a fully interactive land-surface model (Rieck *et al.*, 2014; Xiao *et al.*, 2018). Here, for simplicity, a checkerboard pattern is chosen. For the majority of this article two configurations are used, one with a patch size of 51.2 km (representing the size of a typical GCM grid box) and another with a patch size of 12.8 km (representing the size of a typical global NWP grid box). These simulations are henceforth referred to as M-P50 and M-P12, respectively.

The functional form of the surface fluxes is identical for each patch, with a half-sine wave for 12 hr followed by zero fluxes for 12 hr as in M-CON, but the amplitudes of the half-sine waves differ. The patches labelled DRY have peak values of sensible and latent heat fluxes of 250 and $280\,\mathrm{W{\cdot}m^{-2}}$ respectively, whereas the patches labelled WET have peak sensible and latent fluxes of 90 and $440\,\mathrm{W{\cdot}m^{-2}}$. These choices mean that the total surface flux is the same within each patch but the partitioning differs, with the Bowen ratio alternating between 0.2 and 0.9. Our focus on variations in the partitioning, and the association of warm (cold) with dry (wet) surface flux anomalies, is consistent with the observations of Mahrt (1991) for scales of order 10 km. Our choices also result in a larger domain-mean Bowen ratio for the heterogeneous configurations than M-CON. To aid with the comparisons, further companion simulations have been performed with spatially homogeneous surface flux conditions matching the WET (M-WET)

TABLE 1 Summary of the domain size, patch size, horizontal grid spacing, how convection is treated and the maximum values of latent (L) and sensible (H) heat flux in all of the simulations analysed in this study

Simulation	Domain size (km)	Patch size (km)	Horizontal grid spacing (km)	Parameterised convection?	Maximum H ($W \cdot m^{-2}$)	Maximum L ($W \cdot m^{-2}$)
M-CON	102.4 × 102.4	HOM	0.2	No	130	400
M-WET	51.2 × 51.2	HOM	0.2	No	90	440
M-DRY	51.2 × 51.2	HOM	0.2	No	250	280
M-P50	102.4 × 102.4	1.2	0.2	No	90/250	440/280
M-P12	102.4 × 102.4	12.8	0.2	No	90/250	440/280
UM-G24	192 × 192	HOM	24	Yes	130	400
UM-G12	192 × 192	HOM	12	Yes	130	400
UM-G06	192 × 192	HOM	6	Yes	130	400
UM-P48G24	192 × 192	48	24	Yes	90/250	440/280
UM-P48G12	192 × 192	48	12	Yes	90/250	440/280
UM-P48G06	192 × 192	48	6	Yes	90/250	440/280
UM-P12G12	192 × 192	12	12	Yes	90/250	440/280
UM-P12G06	192 × 192	12	6	Yes	90/250	440/280

and DRY (M-DRY) patches. M-WET and M-DRY have a smaller domain size (51.2 km × 51.2 km) than M-CON in order to match them with the heterogeneous patch size in M-P50. However, in additional experiments not shown here, it was established that results to be presented for the homogeneous simulations are not sensitive to domain size.

2.3.2 | Simulations with parameterised convection

The simulation domain used for the idealised MetUM simulations is $(192\,km)^2$. The numbers of grid points used are 8 × 8, 16 × 16, and 32 × 32, giving grid spacings of 24 km (G24), 12 km (G12), and 6 km (G06), respectively. The model time step is varied with resolution from 15 min for a grid spacing of 24 km to 2.5 min for 6 km. The patch sizes used for the tiling of WET and DRY are 12 km (P12) and 48 km (P48). As in the high-resolution MONC simulations, the surface heat fluxes are varied sinusoidally, with the peak values 6 hr after the start of the forcing, and the same cooling profile is applied (Figure 1c).

Each MetUM simulation is run for 10 days, with analysis presented from the last 9 days to avoid issues with model spin-up. As in the high-resolution simulations, companion simulations with no imposed surface heterogeneity are also performed. These simulations have the same domain as the simulations with surface heterogeneity. A full list of the simulations considered is provided in Table 1.

3 | THE EVOLUTION OF CONVECTION IN THE HIGH-RESOLUTION MONC SIMULATIONS

3.1 | Domain-mean precipitation and cross-patch circulations

Figure 2a shows the domain-mean precipitation rate for the two patch experiments (M-P50 and M-P12), the smaller domains with uniform surface forcing (M-DRY, M-WET), and M-CON. The zero time corresponds to 24 hr into the simulation, at the start of the second period of surface forcing. The simulations with surface heterogeneity initiate precipitation approximately 2.5 hr after start of the surface forcing, with a peak in precipitation occurring one hour later. The simulations with homogeneous surface conditions (M-CON, M-DRY, and M-WET) produce a precipitation peak approximately one hour later again, at 4.5 hr after the start of surface forcing. M-DRY and M-WET initiate their first precipitation after approximately 3 hr. In all of the simulations, the first precipitation occurs within the range of initiation times found in diurnal cycles 2–10 of the M-CON simulation. As the surface forcing decreases (beyond hour 6), the precipitation rates in all of the simulations decay and the precipitation stops shortly after the surface forcing ends at hour 12. The domain-mean daily-mean precipitation rates for the simulations with surface heterogeneity are very similar to those of M-CON, balancing with the total imposed forcing.

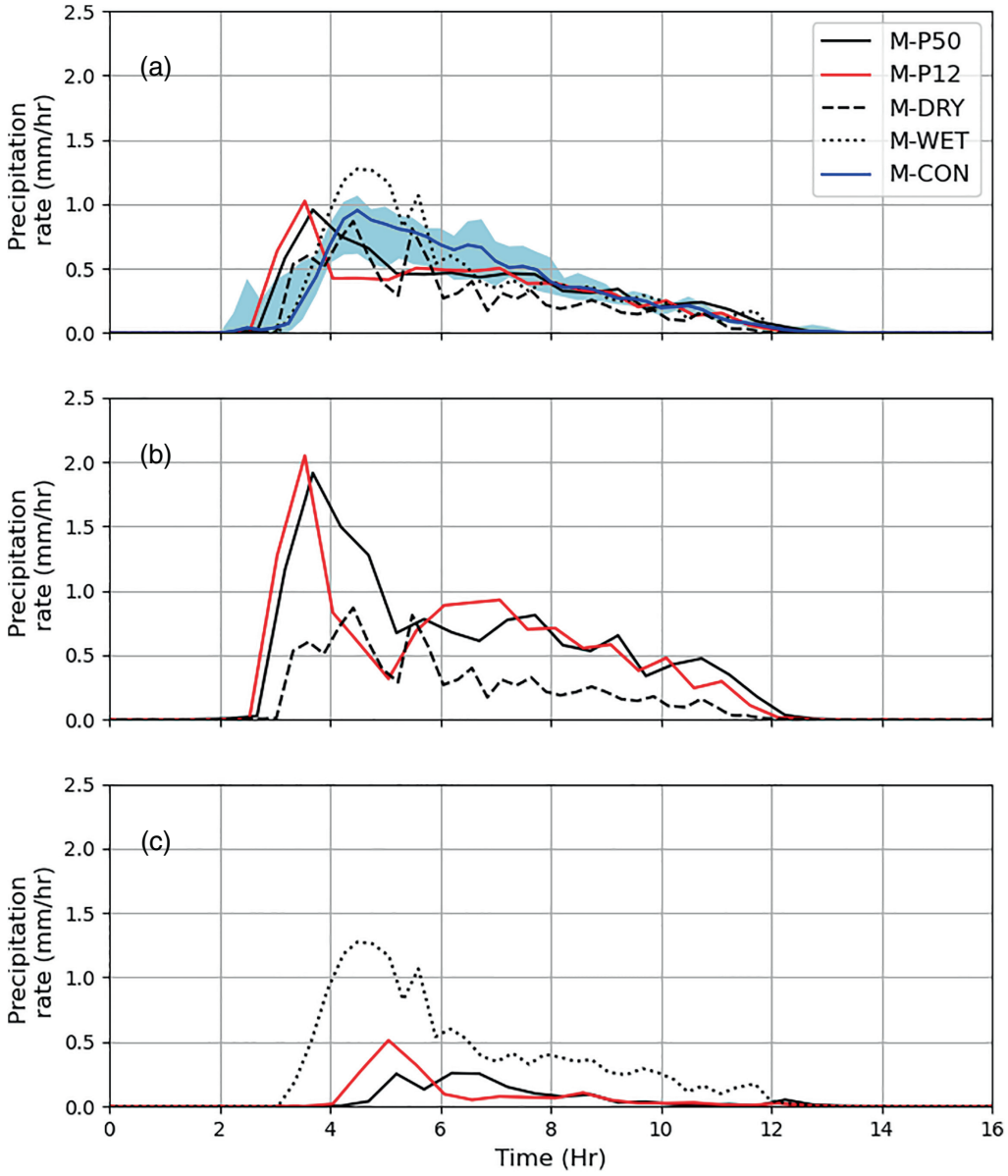

FIGURE 2 The time evolution of spatial-mean surface precipitation in the high-resolution simulations, for averages over (a) the whole domain, (b) just the DRY patches, and (c) just the WET patches. The evolutions from the M-DRY and M-WET homogeneous MONC simulations are shown with dashed and dotted lines, respectively. The blue shading indicates the range of precipitation rates across days 2–10 of M-CON. The domain-mean daily-mean precipitation on day 2 is 0.16, 0.21, and 0.25 mm·h^{-1} for M-WET, M-CON, and M-DRY, respectively

Precipitation over the DRY patches occurs earlier than that over the WET patches by 1.5 hr (Figure 2b,c) in both the M-P50 and M-P12 simulations. The precipitation over the DRY patches is also much stronger than that over the WET patches (by more than 400% at the times of their respective peak precipitation). Also, the peak precipitation rates within the DRY patches are double those in M-CON. The WET patches initiate precipitation approximately an hour after M-CON and have much less precipitation. These points highlight the strong impacts that surface heterogeneity can have on local precipitation rates and timings. There may be a relationship between patch size and the timing of peak precipitation (M-P12 peaks just before M-P50), but it is not possible to show this robustly using the simulations available in this study (cf. Rieck *et al.*, 2014).

The heterogeneity provides a source for increased low-level variability, and it is interesting to note that the change in the time of peak precipitation between the heterogeneously and homogeneously forced simulations is comparable with that found in Stirling and Petch (2004), when the variability in temperature and moisture was increased in the boundary layer. Stirling and Petch (2004) also found that rainfall amounts could change by 70%.

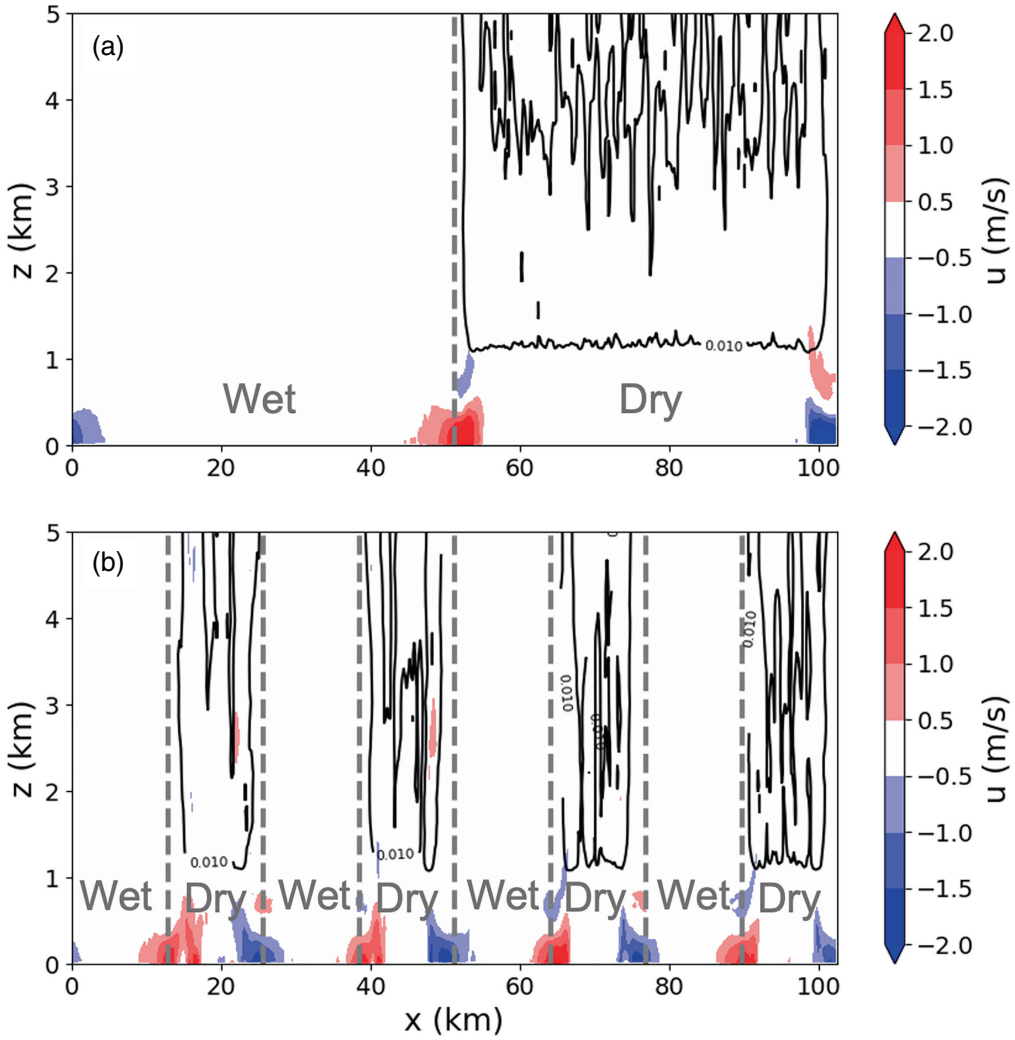

FIGURE 3 Vertical cross-section of mean liquid water (the solid black contour denotes 0.01 g·kg^{-1}) and mean horizontal wind (filled contours) for (a) M-P50 and (b) M-P12, 2.7 hr after the start of surface forcing. In each case, values are averaged in the y-direction across the row of patches that starts at $y = 51.2$ km. Dashed vertical lines indicate the location of patch boundaries

However, because the studied regime is one for which the daily-mean domain-mean precipitation balances with the imposed forcing, no increase in domain-mean rainfall totals is seen in the high-resolution simulations performed here.

Figure 3 shows the mesoscale circulations in the x-direction that develop due to the surface heterogeneity. Differential heating patterns at the surface generate horizontal pressure gradients, which induce flow from the cool/wet to the warm/dry surfaces. Locations with a sharp horizontal gradient in u show the position of the breeze front. In the simulations presented here, the maximum horizontal flow is approximately 2 m·s^{-1}, which is similar to that found in Rieck *et al.* (2014). Cloud development is enhanced at the leading edge of the front where air is lifted (as in, e.g., Garcia-Carreras *et al.*, 2011). This is particularly pronounced 2 hr after the start of the surface forcing and leads to the formation of the first clouds along the sea-breeze-like front induced by the differences between the surface properties of the patches (not shown). Thus, the development of these mesoscale circulations is responsible for the earlier initiation of precipitation within the DRY patches in the heterogeneous simulations.

The low-level convergence into the DRY patches is also demonstrated by Figure 4, which shows the transport across the patch boundaries for the M-P50 and M-P12 simulations. The magnitude of the transport is larger in the M-P12 simulation with the smaller patch size. After approximately 3.5 hr, the circulation at 169 m switches sign, indicating convergence into the WET patches for both M-P12 and M-P50, although M-P12 transitions before M-P50. By this time, deep convection is well developed over the DRY patches, and the deep convective circulations generate outflow and cold pools within the boundary layer (not shown). Due to the earlier development and enhanced convection over the DRY patches, the overall effect is to cool the boundary layer and produce a superposition of convective outflows that causes the net low-level flow across the boundary to reverse. Again the magnitude of the circulation is largest in the M-P12 simulation. At later times, once deep convection

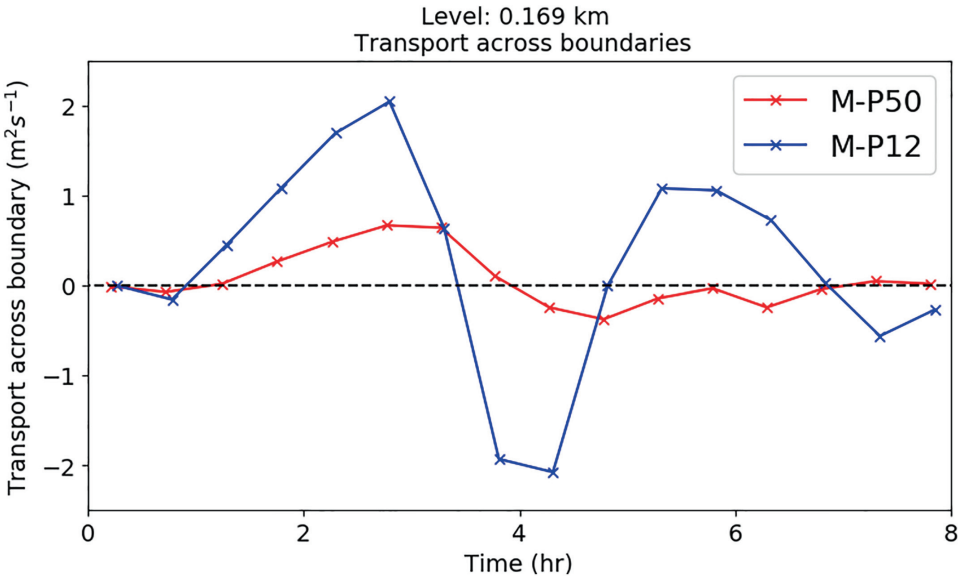

FIGURE 4 Time evolution of transport from wet to dry patches across the boundaries of the DRY and WET patches for M-P50 (red) and M-P12 (blue) at a height of 169 m. The transport is obtained from $\oint \mathbf{u}.\mathbf{d}\ell$, where $\mathbf{d}\ell$ is normal to the patch boundary and directed towards the adjacent DRY patch

has become established within both sets of patches, there are low-level cold-pool outflows across the boundaries in both senses. A coherent circulation signal is re-established between hours 5 and 7 in MP-12, which is forced by differential heating between the DRY and WET patches (Figure 5c).

The signature of the circulation switch can also be seen in Figure 5, which shows time–height cross-sections of the mean differences between the DRY and WET patches for three atmospheric variables in the M-P12 simulation. Also marked on the figure are the heights of the inversion for the two patches, defined from the maximum in the second derivative of potential temperature. The circulation change is most evident in the patch difference in the mean vertical velocity (Figure 5a), for which variable the differences extend throughout the troposphere (heights above 5 km not shown). Associated changes of sign can also be seen in the patch differences in potential temperature (Figure 5c), although these differences are largely confined within the well-mixed part of the boundary layer. Differences in the water vapour (Figure 5b) are more consistent in time. *Above the boundary layer, ascent acts to cool and moisten the atmosphere over the DRY patches (and vice versa over the WET patches), these tendencies being offset by the enhanced deep convective activity over the patches. The net effect is to adjust the patch-scale free-tropospheric state in the direction of the additional convective forcing, so that the DRY patches above the boundary layer are more cooler and more* moist than the WET patches. The slight initial moisture difference at the start of the forcing is caused by the differences in convective activity from the previous day of the simulations. Similar vertical structures for the patch differences were also found in the M-P50 simulations (not shown).

3.2 | What is the spatial distribution of the surface precipitation?

As discussed above, larger amounts of precipitation fall on the DRY patches. Figure 6 shows the spatial distribution of accumulated precipitation for 8 hr after the surface forcing starts in both the M-P50 and M-P12 simulations. The distinction between the WET and DRY patches is very clear in both simulations, although the boundary edges of the patches are less readily apparent in M-P12.

To assess the impact of patch size more systematically, Figure 7 shows the accumulated precipitation composite for WET and DRY patches, while Figure 8 shows the precipitation as a function of distance from the patch edges. In the M-P50 simulation, the precipitation does not have strongly preferred locations within the WET patches (Figures 7a and 8a). In the DRY patches, there is enhanced rainfall at the centre of the patch, and also around 2.5–5 km into the patch, where the first convective cells are triggered by the low-level circulation (Figure 3a). In the M-P12 simulation, there is some preference for precipitation to fall at the centre or along the edges of the WET patches (Figures 7c and 8b) and a clear preference in the DRY patches for precipitation to increase towards the centre (Figures 7d and 8b). A peak at around 3 km from the edge of the DRY patches corresponds to the distance at which there is reduced precipitation in the WET patches and is consistent with the propagation of the low-level circulation at the time when the first, and strongest, convection develops. Precipitation in the DRY patches also extends somewhat into the adjoining WET patches, particularly at the corners.

Aspects of these distributions can be interpreted in terms of the spatial distribution of 200-m vertical velocity,

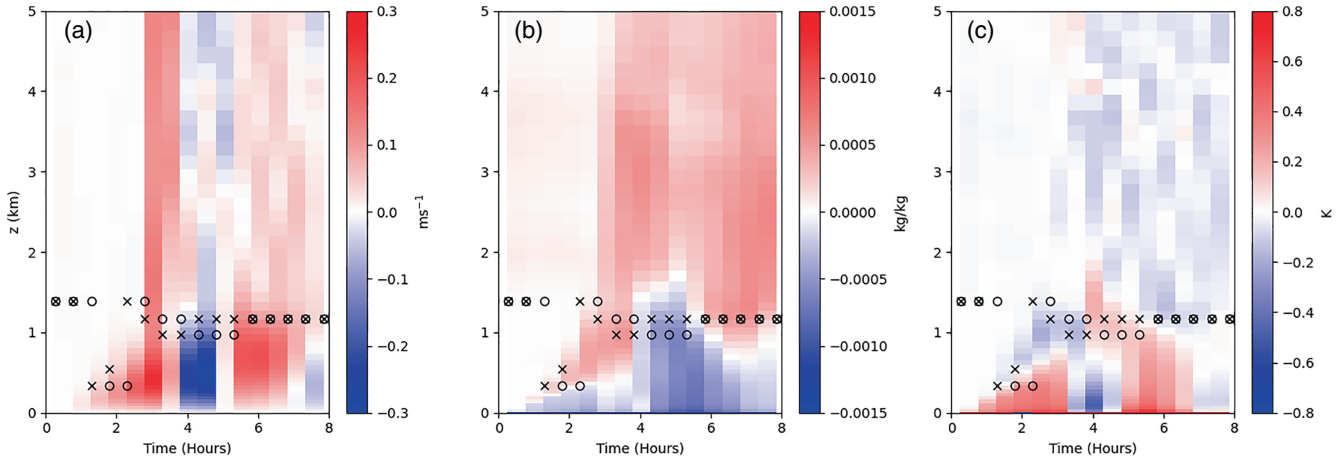

FIGURE 5 Time–height sections of differences between the mean properties of the DRY and WET patches for (a) vertical velocity, (b) water vapour, and (c) potential temperature for the M-P12 simulation. Black crosses indicate the potential temperature inversion height diagnosed from patch-mean profiles over the DRY patches and black circles indicate the corresponding inversion height for the WET patches

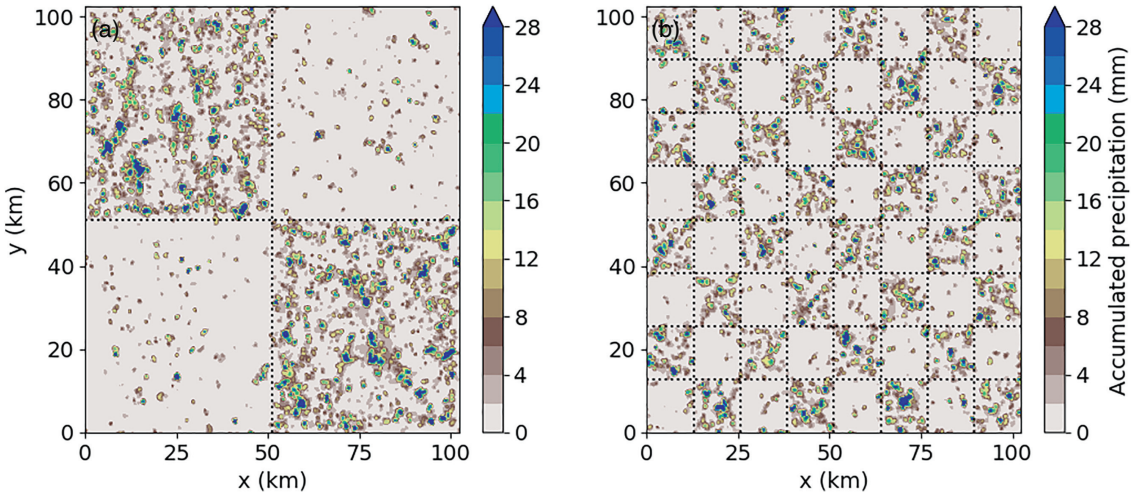

FIGURE 6 The spatial distribution of precipitation in the (a) M-P50 and (b) M-P12 simulations. Accumulations are presented for the first 8 hr after the start of forcing on the second day of each simulation. In each case a DRY patch is found in the top left corner. The dotted lines indicate the patch boundaries

as shown in Figure 9 for 2.7 hr after the start of surface forcing. In the M-P50 simulation, the sizes of the developing convective cells in the WET and DRY patches are similar, but the magnitude of the overturning is larger in the DRY patches. There are relatively small vertical velocities around the edges of the DRY patches (co-located with the smaller aggregated precipitation rates) behind propagating frontal features that mark the low-level circulation. There are also diagonal bands of high vertical velocity (>4 $m \cdot s^{-1}$) that occur in the DRY patches, where the circulations associated with adjacent edges meet each other. These bands pass through the corners of the patches and hence provide a link between the DRY areas. The M-P12 simulation presents some similar features, but the concentration of convection within the centre of the DRY patches leads to a small square of enhanced convection. Locations of strong descent with associated developing cold pools are also apparent in this simulation, especially towards the edge and corners of the DRY patches where other circulations meet. The structures shown here become somewhat less marked after approximately 3.5 hr, due to the continuing action of deep convection.

4 | THE EVOLUTION OF CONVECTION IN THE IDEALISED METUM SIMULATIONS

Section 3 describes the impact of surface heterogeneity on the evolution of spatial mean precipitation rate,

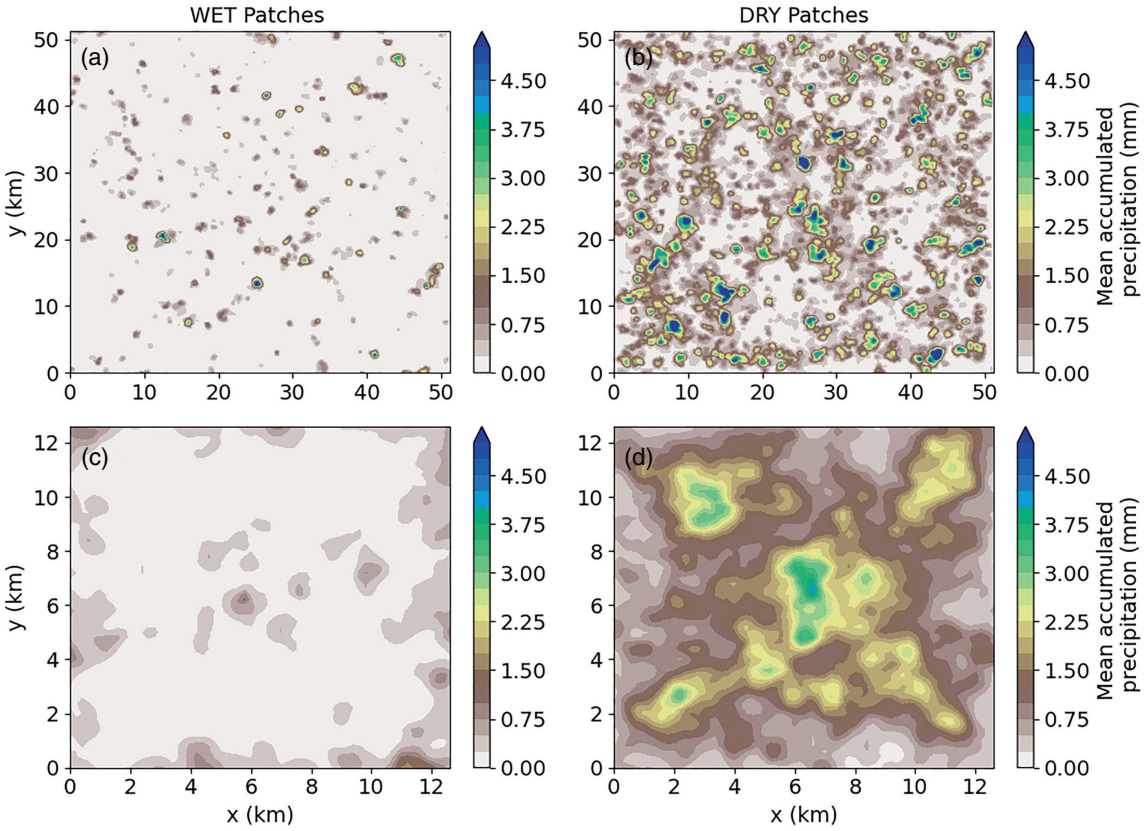

FIGURE 7 Composite spatial precipitation distributions averaged over all (a, c) WET and (b, d) DRY patches in the (a, b) M-P50 and (c, d) M-P12 simulations

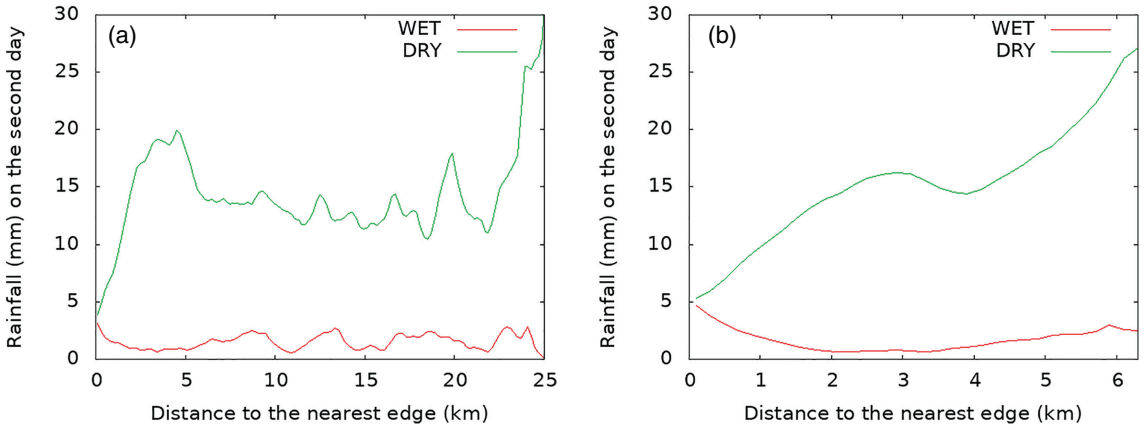

FIGURE 8 Precipitation within the WET (red) and DRY (green) patches as a function of distance from the nearest patch edge. All edge points have distance zero, while the centre point has a distance corresponding to half the patch size. The precipitation is accumulated over time for the second day and is averaged over all contributing grid points for the given distance. (a) M-P50 simulation and (b) M-P12

local circulations, and the spatial distribution using a high-resolution cloud-resolving model. In this section the same analysis is applied to examine the companion simulations with parameterised convection performed using the idealised configuration of the MetUM. The aim is to assess whether simulations of the diurnal cycle of deep convection with parameterised convection are able to produce a similar response to the surface heterogeneity.

Figure 10 shows the evolution of precipitation over the whole domain with heterogeneous surface forcing (Figure 10a), the whole domain with homogeneous surface forcing (Figure 10b), and over the DRY patches (Figure 10c) and WET patches (Figure 10d) for the eight

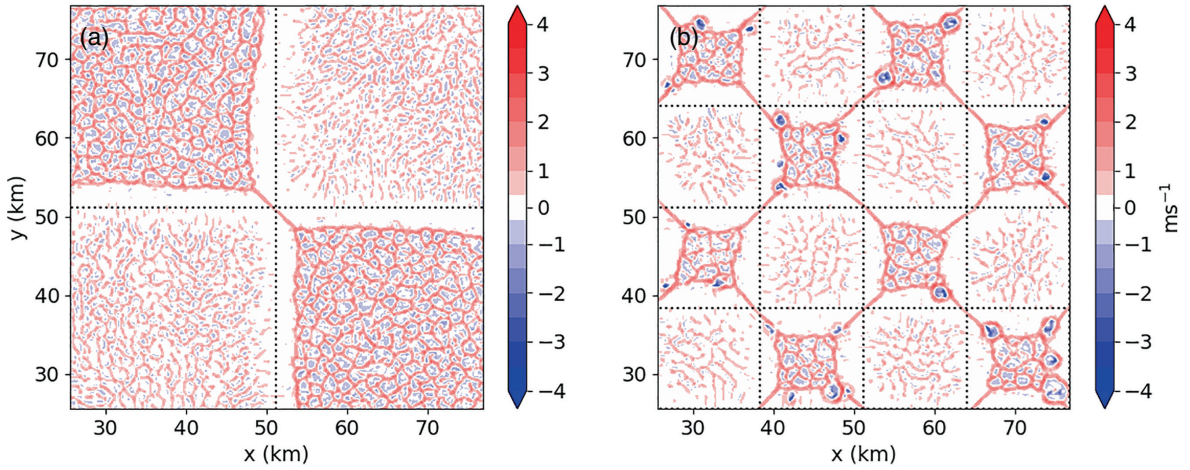

FIGURE 9 Plan view of vertical velocity at 200 m above the surface for the centre of the computational domain at 2.7 hr after the start of surface forcing for (a) M-P50 and (b) M-P12. The dotted lines indicate the patch boundaries

simulations performed using the idealised MetUM (five with heterogeneous surface forcing and three with homogeneous surface forcing). Also shown is the evolution of the MONC reference simulations M-CON, M-DRY, and M-WET. The shading indicates the range in precipitation rates over the last 9 days of the simulations. Qualitatively, the simulations with heterogeneous patches have similar domain-mean precipitation evolutions to those of the high-resolution simulations M-P50 and M-P12 (Figure 2). As in the high-resolution simulations, precipitation over the DRY patches is much larger (here by up to ten times) than over the WET patches. Peak local values of precipitation rate in the MetUM (not shown) are larger than those in high-resolution M-P50 simulation by approximately a factor of four. The DRY patch precipitation starts approximately 1 hr after the surface forcing starts (Figure 10c), which is approximately 1.5 hr earlier than in the high-resolution simulations (Figure 2b). The precipitation is a little delayed in the mean for the 48-km patches relative to the 12-km patches, and consistent with the sense of the patch size differences in MONC (Figure 2b). However, some caution is needed in interpreting those differences, given the timing variations seen for different days of the MetUM *and MONC* simulations. The wet patch precipitation starts at approximately 2.25 hr after the start of the surface forcing (Figure 10d), which is approximately 1.75 hr earlier than in the wet patches of the high-resolution simulations with heterogeneous forcing (Figure 2c), but similar to the time of initiation of precipitation in the homogeneous high-resolution simulations with MONC. The evolution of the convection is similar over both patch types: an initial peak with a rapid reduction in precipitation rate, followed by a more gradual decay in line with the reduction in surface forcing. The homogeneous MetUM simulations (Figure 10b) initiate precipitation approximately 2 hr after the start of surface forcing and produce no immediate peak. Rather, there is a much slower increase in precipitation rate and the peak is delayed with respect to high-resolution homogeneous simulations. The peak of the domain-mean precipitation rate in homogeneous parameterised simulations UM-G06 and UM-G12 is comparable to that in M-CON ($\sim$1 mm·h^{-1}) but is delayed by approximately 2 hr, while that in UM-G24 is smaller ($\sim$0.75 mm·h^{-1}) and is delayed by approximately *0.75* hr or occurs approximately *1.25* hr earlier than in UM-G06 and UM-G12. This latter result suggests that reducing horizontal grid spacing may not by itself improve the ability of the MetUM to capture the timing of diurnal cycle of convection.

In the simulations performed using the idealised MetUM, there is little indication of any coherent mesoscale circulations having developed at the boundaries of the patches. (We tested this statement by calculating the cross-patch transport as in Figure 4.) In part, this will reflect the earlier initiation of precipitation, which means that there is less time for the differential surface heating to develop a low-level circulation, and in part it will reflect the difficulty in being able to resolve any such circulation adequately. Thus, the rainfall characteristics of the patches are not driven by a low-level dynamical forcing, but rather are dominated by the evolution of differences in the thermodynamic profiles. The differences between the patches are illustrated by Figure 11, which is the same as Figure 5 but for the second day of the simulation UM-P12G12. A vertical velocity difference develops after precipitation initiates (approximately 2 hr after forcing starts) with descent over the DRY patches, which is opposite to the difference at the corresponding time in M-P12 (Figures 5a and 11a). There is also a weak signal of a near-surface potential temperature reversal between the DRY and WET patches

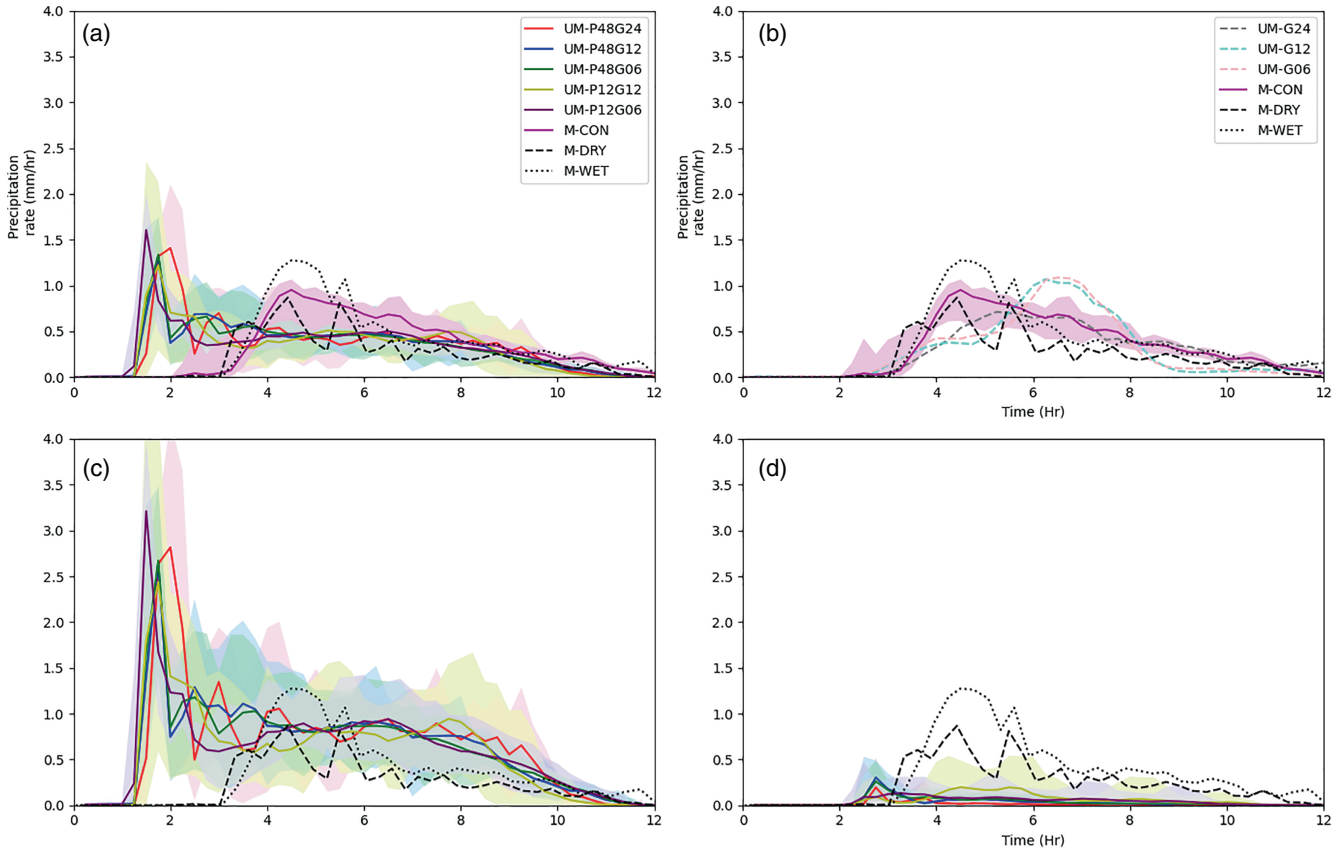

FIGURE 10 The time evolution of spatial-mean surface precipitation in the idealised MetUM simulations with parameterised convection. Results are shown for averages over (a) the whole domain for the heterogeneous MetUM forcing cases, (b) the whole domain for the homogeneous MetUM forcing cases, (c) the DRY patches of the heterogeneous MetUM forcing cases, and (d) the WET patches of the heterogeneous forcing cases. The solid curves represent the mean, while the shading indicates the range of precipitation rates across days 2–10 of the MetUM simulations. In each panel, for comparison purposes, the results are also shown for the domain mean of high-resolution MONC simulations with homogeneous forcing

between hours 5 and 7 (Figure 11c), which may be compared with the reversal between hours 3 and 5 in the MONC simulation M-P12 (Figure 5c). Another feature of the MetUM simulation is that it exhibits a stronger moisture difference between the patches within the free troposphere (Figures 5b and 11b). The contrast between MONC and the MetUM is particularly notable at the start of the surface forcing. The free-tropospheric moisture difference has the opposite sign to that within the boundary layer and is a consequence of the *stronger precipitation (hence greater moistening due to detrainment from deep convection)* within the DRY patches on the previous day. It is also a contributing factor that supports that precipitation difference on the following day. Similar behaviour is present in all of the simulations with parameterised convection with imposed surface heterogeneity.

The potential temperature profile develops a near-surface inversion associated with the imposed nocturnal cooling, which is eroded by positive surface sensible heat fluxes prior to the development of moist convection. There is also an inversion at around 1.5 km associated with the daytime boundary layer. The latter is found somewhat higher in the MetUM simulations compared with MONC (Figures 5 and 11) and it is consistently stronger than the near-surface inversion (i.e., it is always picked out by the inversion height diagnostic). The Lock *et al.* (2000) diagnosis of the boundary-layer height nicely picks out the erosion of the near-surface inversion in the MetUM as surface forcing becomes active, and corresponds with the change in sign in the vertical of the patch differences in water vapour and potential temperature (Figure 11b,c).

Figure 12 shows the spatial distribution of the daily-mean precipitation for the simulations with parameterised convection and surface heterogeneity. The distinction between the DRY and WET patches is clear in all of the simulations, but where the model grid size is similar to that of the patch size the response to the patches become less coherent. This may be contrasted with Figure 12c, where the model grid length is an eighth of the patch length and so the patch is resolved. In some of the WET patches

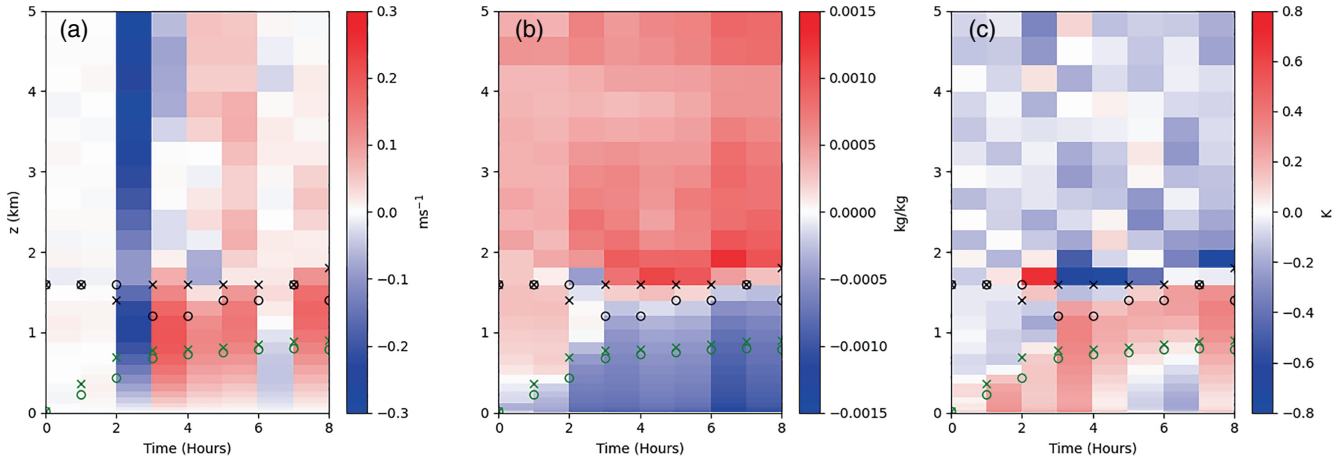

FIGURE 11 Time–height sections of differences between the mean properties of the DRY and WET patches for (a) vertical velocity, (b) water vapour, and (c) potential temperature for day 2 of the UM-P12G12 simulation. Black crosses indicate the potential temperature inversion height diagnosed from patch-mean profiles over the DRY patches and black circles indicate the corresponding inversion height for the WET patches. Green crosses indicate the mean MetUM boundary-layer height diagnostic (Lock *et al.*, 2000) for the DRY patches and green circles indicate the corresponding height for the WET patches. Note that, once convection is active, this metric is set to equal the lifting condensation level (LCL)

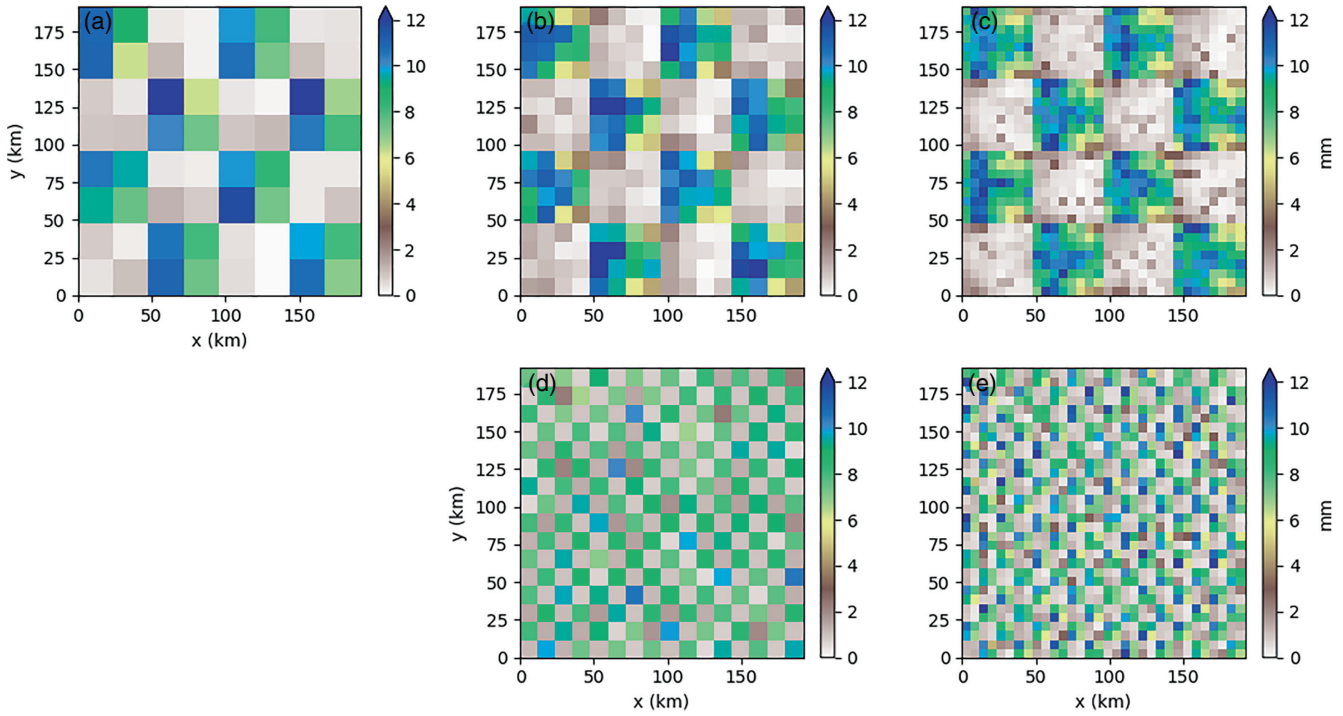

FIGURE 12 The spatial distribution of the daily-accumulated precipitation in the (a) UM-P48G24, (b) UM-P48G12, (c) UM-P48G06, (d) UM-P12G12, and (e) UM-P12G06 simulations. In each case a DRY patch is found in the top left corner. Results are averaged over days 2 to 10 of the MetUM simulations

on this panel, there are individual grid boxes of slightly higher precipitation rates and in a number of DRY patches there are regions at the edge of the patch with lower precipitation rates. Such observations can also be made in Figure 12b, albeit to a lesser extent. These points suggest that it is possible to capture some signals of the spatial distribution of precipitation, even though the convection is parameterised and the patch resolution may be poor. The fractions of domain-mean precipitation in WET and DRY patches of the high-resolution MONC simulations M-P50 and MP12 and all the MetUM simulations performed in this study are shown in Table 2. For the high-resolution

TABLE 2 Fraction of domain-mean precipitation for grid boxes that are WET and DRY for the high-resolution MONC simulations and all the idealised MetUM simulations

Simulations	DRY patches	WET patches
M-P50	0.90	0.10
M-P12	0.87	0.13
UM-P48G24	0.94	0.06
UM-P48G12	0.91	0.09
UM-P48G06	0.91	0.09
UM-P12G12	0.88	0.12
UM-P12G06	0.89	0.11

MONC simulations, approximately 90% of the precipitation falls in the DRY patches regardless of the patch size. A similar result is obtained in all the MetUM simulations, suggesting that patch size and grid resolution do not influence the location of precipitation on the patch scale in simulations with parameterised convection.

5 | SUMMARY AND CONCLUSIONS

This study investigates the impact of idealised surface heterogeneity on the diurnal cycle of deep convection using simulations performed using a high-resolution cloud-resolving model (MONC) and the idealised configuration of the Met Office UM with parameterised convection. Companion homogeneously forced simulations using both models initiate precipitation at approximately the same time, but with the precipitation rates reaching their maximum earlier in MONC. For both models, the development of convection responds to the inclusion of surface heterogeneity. The heterogeneously forced high-resolution simulations (M-P50 and M-P12) initiate precipitation within the range of initiation times found in the homogeneously forced high-resolution simulations. Their precipitation rates reach their maximum before the homogeneously forced high-resolution simulations, and they have peak precipitation rates that are comparable with M-CON (1 $mm \cdot hr^{-1}$). For the simulations with parameterised convection, the inclusion of surface heterogeneity results in an earlier triggering of deep convection and an earlier initiation of precipitation for all patch and grid sizes considered here, and also an increase in the peak precipitation rate. Compared with the heterogeneously forced high-resolution simulations, the heterogeneously forced simulations with parameterised convection initiate precipitation at least an hour earlier and have peak precipitation rates that are at least 30% greater. In both the high-resolution and parameterised simulations, differential surface heating causes the precipitation to be tied more closely to the DRY regions in all of the heterogeneously forced simulations studied, with around 90% of the daily-mean precipitation falling in these regions. The ratio between the peak precipitation rates in the DRY and WET patches is around 10 in the parameterised simulations compared with 4–8 in the cloud-resolving simulations. The spatial distribution of precipitation within patches was also considered. Among the high-resolution simulations, heterogeneity within the patches is particularly evident in the M-P12 simulation, where precipitation in the DRY patches has a peak a few km from the edges, while that in the WET patches has a minimum a few km from its edges. There are also some indications of within-patch heterogeneity of precipitation in simulations with parameterised convection, so long as the patch itself can be resolved by the model.

The contrast in precipitation between DRY and WET patches in the parameterised simulations occurs despite the absence of a coherent low-level circulation driven by differential heating prior to the development of convection. The absence may be attributable in part to the lack of resolution of the patches, but is also caused by the earlier triggering of convection in the parameterised simulations before such a circulation can become established. On the other hand, the precipitation contrast in the parameterised simulations is in part self-reinforced through the development of a larger free-tropospheric moisture anomaly over the DRY patches.

These results confirm and expand those in the current literature in demonstrating that surface heterogeneity has the potential to induce impacts on the local timing of precipitation onset and magnitude and the spatial distribution of precipitation, all of which are important factors in forecasting local impacts such as flooding. The parameterised simulations in this case present a mixed picture in reproducing the impacts found in the high-resolution simulations: in general terms, the parameterised model struggles with the aspects of the timing but nonetheless is able to capture aspects of the spatial differences even for marginal patch resolution. Accounting for subgrid heterogeneity through land–atmosphere feedbacks is likely to be an important factor in improving the simulation of the diurnal cycle of convection in climate models, even at coarse horizontal resolution. Natural extensions of this study would be to consider heterogeneity with smoother boundaries (e.g., a sine function as in Kang and Davis (2008)), or to introduce a mean wind or simple vertical wind shear profile to break the symmetry that is present here. The addition of a fully interactive land-surface scheme to MONC could be used to develop and evaluate new parameterisation schemes that take into account surface heteorogeneity and investigate the feedback on the

day-to-day variability of convection over heterogeneous surfaces. Furthermore, the existing high-resolution simulations could be used to evaluate the impact of surface heterogeneity on convective memory (using the memory function introduced by Daleu *et al.* (2020)) or to assess new parameterisation schemes. For example, it would be valuable to assess a scheme such as that of Willett and Whitall (2017), which includes a prognostic entrainment term.

AUTHOR CONTRIBUTIONS

Natalie J. Harvey: conceptualization; data curation; formal analysis; investigation; methodology; visualization; writing – original draft; writing – review and editing. **Chimene L. Daleu:** data curation; investigation; visualization; writing – review and editing. **Rachel A. Stratton:** data curation; writing – original draft; writing – review and editing. **Robert S. Plant:** conceptualization; funding acquisition; investigation; methodology; supervision; visualization; writing – original draft; writing – review and editing. **Steven J. Woolnough:** conceptualization; funding acquisition; investigation; methodology; project administration; supervision; writing – original draft; writing – review and editing. **Alison J. Stirling:** funding acquisition; project administration; supervision; writing – review and editing.

ACKNOWLEDGEMENTS

N.J.H. and S.J.W. gratefully acknowledge funding from NERC Grant NE/M017222/1. C.L.D. and R.S.P. acknowledge funding from NERC Grant NE/N013743/1. S.J.W. was also supported by the National Centre for Atmospheric Science, a NERC collaborative centre, under contract R8/H12/83/001. We acknowledge use of the NEXCS system, a collaborative facility supplied under the Joint Weather and Climate Research Programme, a strategic partnership between the Met Office and the Natural Environment Research Council. We thank three anonymous reviewers for their thorough and constructive comments which have helped to improve the article.

CONFLICT OF INTEREST

The authors declare no conflict of interest. The funders had no role in the design of the study; in the collection, analyses, or interpretation of data; in the writing of the manuscript; or in the decision to publish the results.

ORCID

Natalie J. Harvey https://orcid.org/0000-0003-0973-5794
Chimene L. Daleu https://orcid.org/0000-0003-2075-4902
Rachel A. Stratton https://orcid.org/0000-0001-5795-6247
Robert S. Plant https://orcid.org/0000-0001-8808-0022
Steven J. Woolnough https://orcid.org/0000-0003-0500-8514

REFERENCES

Avissar, R. and Schmidt, T. (1998) An evaluation of the scale at which ground-surface heat flux patchiness affects the convective boundary layer using large-eddy simulations. *Journal of the Atmospheric Sciences*, 55, 2666–2689.

Baur, F., Keil, C. and Craig, G.C. (2018) Soil moisture-precipitation coupling over Central Europe: interactions between surface anomalies at different scales and the dynamical implication. *Quarterly Journal of the Royal Meteorological Society*, 144, 2863–2875. https://doi.org/10.1002/qj.3415.

Bechtold, P., Chaboureau, J.-P., Beljaars, A., Betts, A.K., Köhler, M., Miller, M. and Redelsperger, J.-L. (2004) The simulation of the diurnal cycle of convective precipitation over land in a global model. *Quarterly Journal of the Royal Meteorological Society*, 130, 3119–3137. https://doi.org/10.1256/qj.03.103.

Bechtold, P., Semane, N., Lopez, P., Chaboureau, J.-P., Beljaars, A. and Bormann, N. (2014) Representing equilibrium and nonequilibrium convection in large-scale models. *Journal of the Atmospheric Sciences*, 71, 734–753. https://doi.org/10.1175/JAS-D-13-0163.1.

Birch, C.E., Parker, D.J., Marsham, J.H., Copsey, D. and Garcia-Carreras, L. (2014) A seamless assessment of the role of convection in the water cycle of the West African monsoon. *Journal of Geophysical Research: Atmospheres*, 119, 2890–2912.

Boutle, I.A., Belcher, S.E. and Plant, R.S. (2015) Friction in mid-latitude cyclones: an Ekman-PV mechanism. *Atmospheric Science Letters*, 16, 103–109. https://doi.org/10.1002/asl2.526.

Brown, A.R. (1999) The sensitivity of large-eddy simulations of shallow cumulus convection to resolution and subgrid model. *Quarterly Journal of the Royal Meteorological Society*, 125, 469–482. https://doi.org/10.1002/qj.49712555405.

Brown, A.R., Cederwall, R.T., Chlond, A., Duynkerke, P.G., Golaz, J.-C., Khairoutdinov, M., Lewellen, D.C., Lock, A.P., MacVean, M.K., Moeng, C.-H., Neggers, R.A.J., Siebesma, A.P. and Stevens, B. (2002) Large-eddy simulation of the diurnal cycle of shallow cumulus convection over land. *Quarterly Journal of the Royal Meteorological Society*, 128, 1075–1093.

Brown, N., Weiland, M., Hill, A., Shipway, B., Maynard, C., Allen, T. and Rezny, M. (2015) A highly scalable Met Office NERC Cloud model. *Proceedings of the 3rd International Conference on Exascale Applications and Software*. Edinburgh: University of Edinburgh, pp. 132–137.

Cardoso-Bihlo, E., Khouider, B., Schumacher, C. and De La Chevrotiére, M. (2019) Using radar data to calibrate a stochastic parametrization of organized convection. *Journal of Advances in Modeling Earth Systems*, 11, 1655–1684. https://doi.org/10.1029/2018MS001537.

Christopoulos, C. and Schneider, T. (2021) Assessing biases and climate implications of the diurnal precipitation cycle in climate models. *Geophysical Research Letters*, 48, e2021GL093017. https://doi.org/10.1029/2021GL093017.

Cioni, G. and Hohenegger, C. (2018) A simplified model of precipitation enhancement over a heterogeneous surface. *Hydrology and*

Earth System Sciences, 22, 3197–3212. https://doi.org/10.5194/hess-22-3197-2018.

Clark, A.J., Gallus, W.A. and Chen, T.-C. (2007) Comparison of the diurnal precipitation cycle in convection-resolving and non-convection-resolving mesoscale models. *Monthly Weather Review*, 135, 3456–3473. https://doi.org/10.1175/MWR3467.1.

Colin, M., Sherwood, S., Geoffroy, O., Bony, S. and Fuchs, D. (2019) Identifying the sources of convective memory in cloud-resolving simulations. *Journal of the Atmospheric Sciences*, 76, 947–962. https://doi.org/10.1175/JAS-D-18-0036.1.

Courault, D., Drobinski, P., Brunet, Y., Lacarrere, P. and Talbot, C. (2007) Impact of surface heterogeneity on a buoyancy-driven convective boundary layer in light winds. *Boundary-Layer Meteorology*, 124, 383–403.

Dai, A. (2006) Precipitation characteristics in eighteen coupled climate models. *Journal of Climate*, 19, 4605–4630. https://doi.org/10.1175/JCLI3884.1.

Daleu, C.L., Plant, R.S., Woolnough, S.J., Stirling, A.J. and Harvey, N.J. (2020) Memory properties in cloud-resolving simulations of the diurnal cycle of deep convection. *Journal of Advances in Modeling Earth Systems*, 12, e2019MS001897. https://doi.org/10.1029/2019MS001897.

Davies, L., Plant, R.S. and Derbyshire, S.H. (2009) A simple model of convection with memory. *Journal of Geophysical Research: Atmospheres*, 114, D17202. https://doi.org/10.1029/2008JD011653.

Dearden, C., Hill, A., Coe, H. and Choularton, T. (2018) The role of droplet sedimentation in the evolution of low-level clouds over southern West Africa. *Atmospheric Chemistry and Physics*, 18, 14253–14269. https://doi.org/10.5194/acp-18-14253-2018.

Dipankar, A., Webster, S., Sun, X., Snachez, C., North, R., Furtado, K., Wilkinson, J., Lock, A., Vosper, S., Huang, X.-Y. and Barker, D. (2020) SINGV: a convective-scale weather forecast model for Singapore. *Quarterly Journal of the Royal Meteorological Society*, 146, 4131–4136. https://doi.org/10.1002/qj.3985.

Dirmeyer, P.A., Cash, B.A., Kinter, J.L., Jung, T., Marx, L., Satoh, M., Stan, C., Tomita, H., Towers, P., Wedi, N., Achuthavarier, D., Adams, J.M., Altshuler, E.L., Huang, B., Jin, E.K. and Manganello, J. (2012) Simulating the diurnal cycle of rainfall in global climate models: resolution versus parameterization. *Climate Dynamics*, 39, 399–418. https://doi.org/10.1007/s00382-011-1127-9.

Fast, J.D., Berg, L.K., Alexander, L., Bell, D., D'Ambro, E., Hubbe, J., Kuang, C., Liu, J., Long, C., Matthews, A., Mei, F., Newsom, R., Pekour, M., Pinterich, T., Schmid, B., Schobesberger, S., Shilling, J., Smith, J.N., Springston, S., Suski, K., Thornton, J.A., Tomlinson, J., Wang, J., Xiao, H. and Zelenyuk, A. (2019) Overview of the HI-SCALE field campaign: a new perspective on shallow convective clouds. *Bulletin of the American Meteorological Society*, 100, 821–840. https://doi.org/10.1175/BAMS-D-18-0030.1.

Garcia-Carreras, L., Parker, D.J. and Marsham, J.H. (2011) What is the mechanism for the modification of convective cloud distributions by land surface-induced flows? *Journal of the Atmospheric Sciences*, 68, 619–634. https://doi.org/10.1175/2010JAS3604.1.

Garcia-Carreras, L., Parker, D.J., Taylor, C.M., Reeves, C.E. and Murphy, J.G. (2010) Impact of mesoscale vegetation heterogeneities on the dynamical and thermodynamic properties of the planetary boundary layer. *Journal of Geophysical Research: Atmospheres*, 115, D03102. https://doi.org/10.1029/2009JD012811.

Gerard, L. and Geleyn, J.-F. (2005) Evolution of a subgrid deep convection parametrization in a limited-area model with increasing resolution. *Quarterly Journal of the Royal Meteorological Society*, 131, 2293–2312. https://doi.org/10.1256/qj.04.72.

Gregory, D. and Rowntree, P.R. (1990) A mass flux convection scheme with representation of cloud ensemble characteristics and stability-dependent closure. *Monthly Weather Review*, 118, 1483–1506.

Grosvenor, D.P., Field, P.R., Hill, A.A. and Shipway, B.J. (2017) The relative importance of macrophysical and cloud albedo changes for aerosol-induced radiative effects in closed-cell stratocumulus: insight from the modelling of a case study. *Atmospheric Chemistry and Physics*, 17, 5155–5183. https://doi.org/10.5194/acp-17-5155-2017.

Gu, J.-F., Plant, R.S., Holloway, C.E., Jones, T.R., Stirling, A., Clark, P.A., Woolnough, S.J. and Webb, T.L. (2020) Evaluation of the bulk mass flux formulation using large-eddy simulations. *Journal of the Atmospheric Sciences*, 77, 2115–2137. https://doi.org/10.1175/JAS-D-19-0224.1.

Guichard, F., Petch, J.C., Redelsperger, J.-L., Bechtold, P., Chaboureau, J.-P., Cheinet, S., Grabowski, W., Grenier, H., Jones, C.G., Köhler, M., Piriou, J.-M., Tailleux, R. and Tomasini, M. (2004) Modelling the diurnal cycle of deep precipitating convection over land with cloud-resolving models and single-column models. *Quarterly Journal of the Royal Meteorological Society*, 130, 3139–3172.

Hagos, S., Feng, Z., Plant, R.S. and Protat, A. (2020) A machine learning assisted development of a model for the populations of convective and stratiform clouds. *Journal of Advances in Modeling Earth Systems*, 12, e2019MS001798. https://doi.org/10.1029/2019MS001798.

Hill, A.A., Shipway, B.J. and Boutle, I.A. (2015) How sensitive are aerosol-precipitation interactions to the warm rain representation? *Journal of Advances in Modeling Earth Systems*, 7, 987–1004. https://doi.org/10.1002/2014MS000422.

Hohenegger, C. and Stevens, B. (2013) Controls on and impacts of the diurnal cycle of deep convective precipitation. *Journal of Advances in Modeling Earth Systems*, 5, 801–815. https://doi.org/10.1002/2012MS000216.

Huang, H.-Y. and Margulis, S.A. (2009) On the impact of surface heterogeneity on a realistic convective boundary layer. *Water Resources Research*, 45, W04425. https://doi.org/10.1029/2008WR007175.

Kang, S.-L. and Davis, K.J. (2008) The effects of mesoscale surface heterogeneity on the fair-weather convective atmospheric boundary layer. *Journal of the Atmospheric Sciences*, 65, 3197–3213.

Kang, S.-L., Davis, K.J. and LeMone, M. (2007) Observations of the ABL structures over a heterogeneous land surface during IHOP_2002. *Journal of Hydrometeorology*, 8, 221–244. https://doi.org/10.1175/JHM567.1.

Kealy, J.C., Efstathiou, G.A. and Beare, R.J. (2019) The onset of resolved boundary-layer turbulence at grey-zone resolutions. *Boundary-Layer Meteorology*, 171, 31–52. https://doi.org/10.1007/s10546-018-0420-0.

Khairoutdinov, M., Randall, D. and DeMott, C. (2005) Simulations of the atmospheric general circulation using a cloud-resolving model as a superparameterization of physical processes. *Journal of the Atmospheric Sciences*, 62, 2136–2154. https://doi.org/10.1175/JAS3453.1.

Kirshbaum, D.J. and Fairman, J.G. (2015) Cloud trails past the lesser Antilles. *Monthly Weather Review*, 143, 995–1017.

Kooperman, G.J., Pritchard, M.S., Burt, M.A., Branson, M.D. and Randall, D.A. (2016) Robust effects of cloud superparameterization on simulated daily rainfall intensity statistics across multiple versions of the Community Earth System Model. *Journal of Advances in Modeling Earth Systems*, 8, 140–165. https://doi.org/10.1002/2015MS000574.

Lee, J.M., Zhang, Y. and Klein, S.A. (2019) The effect of land surface heterogeneity and background wind on shallow cumulus clouds and the transition to deeper convection. *Journal of the Atmospheric Sciences*, 76, 401–419. https://doi.org/10.1175/JAS-D-18-0196.1.

Lee, M.-I., Schubert, S.D., Suarez, M.J., Schemm, J.-K.E., Pan, H.-L., Han, J. and Yoo, S.-H. (2008) Role of convection triggers in the simulation of the diurnal cycle of precipitation over the United States Great Plains in a general circulation model. *Journal of Geophysical Research: Atmospheres*, 113, D02111. https://doi.org/10.1029/2007JD008984.

Liu, C. and Zipser, E.J. (2008) Diurnal cycles of precipitation, clouds, and lightning in the tropics from 9 years of TRMM observations. *Geophysical Research Letters*, 36, L04819. https://doi.org/10.1029/2007GL032437.

Lock, A.P., Brown, A.R., Bush, M.R., Martin, G.M. and Smith, R.N.B. (2000) A new boundary layer mixing scheme. Part I: Scheme description and single-column model tests. *Monthly Weather Review*, 128, 3187–3199.

Mahrt, L. (1991) Boundary-layer moisture regimes. *Quarterly Journal of the Royal Meteorological Society*, 117, 151–176. https://doi.org/10.1002/qj.49711749708.

Maronga, B. and Raasch, S. (2013) Large-eddy simulations of surface heterogeneity effects on the convective boundary layer during the LITFASS-2003 experiment. *Boundary-Layer Meteorology*, 146, 17–44.

Marsham, J.H., Blyth, A.M., Parker, D.J., Beswick, K., Browning, K.A., Corsmeier, U., Kalthoff, N., Khodayar, S., Morcrette, C.J. and Norton, E.G. (2007a) Variable cirrus shading during CSIP IOP 5. II: Effects on the convective boundary layer. *Quarterly Journal of the Royal Meteorological Society*, 133, 1661–1675. https://doi.org/10.1002/qj.146.

Marsham, J.H., Dobbie, S. and Hogan, R.J. (2006) Evaluation of a large-eddy model simulation of a mixed-phase altocumulus cloud using microwave radiometer, lidar and Doppler radar data. *Quarterly Journal of the Royal Meteorological Society*, 132, 1693–1715. https://doi.org/10.1256/qj.05.145.

Marsham, J.H., Morcrette, C.J., Browning, K.A., Blyth, A.M., Parker, D.J., Corsmeier, U., Kalthoff, N. and Kohler, M. (2007b) Variable cirrus shading during CSIP IOP 5. I: Effects on the initiation of convection. *Quarterly Journal of the Royal Meteorological Society*, 133, 1643–1660. https://doi.org/10.1002/qj.124.

Marsham, J.H., Parker, D.J., Grams, C.M., Johnson, B.T., Grey, W.M.F. and Ross, A.N. (2008) Observations of mesoscale and boundary-layer scale circulations affecting dust transport and uplift over the Sahara. *Atmospheric Chemistry and Physics*, 8, 6979–6993. https://doi.org/10.5194/acp-8-6979-2008.

McCoy, D.T., Field, P.R., Schmidt, A., Grosvenor, D.P., Bender, F.A.-M., Shipway, B.J., Hill, A.A., Wilkinson, J.M. and Elsaesser, G.S. (2018) Aerosol midlatitude cyclone indirect effects in observations and high-resolution simulations. *Atmospheric Chemistry and Physics*, 18, 5821–5846. https://doi.org/10.5194/acp-18-5821-2018.

Miltenberger, A.K., Field, P.R., Hill, A.A., Rosenberg, P., Shipway, B.J., Wilkinson, J.M., Scovell, R. and Blyth, A.M. (2018) Aerosol–cloud interactions in mixed-phase convective clouds—Part 1: aerosol perturbations. *Atmospheric Chemistry and Physics*, 18, 3119–3145. https://doi.org/10.5194/acp-18-3119-2018.

Nikulin, G., Jones, C., Giorgi, F., Asrar, G., Büchner, M., Cerezo-Mota, R., Christensen, O.B., Déqué, M., Fernandez, J., Hänsler, A., van Meijgaard, E., Samuelsson, P., Sylla, M.B. and Sushama, L. (2012) Precipitation climatology in an ensemble of CORDEX-Africa regional climate simulations. *Journal of Climate*, 25, 6057–6078. https://doi.org/10.1175/JCLI-D-11-00375.1.

Patton, E.G., Sullivan, P.P. and Moeng, C.-H. (2005) The influence of idealized heterogeneity on wet and dry planetary boundary layers coupled to the land surface. *Journal of the Atmospheric Sciences*, 62, 2078–2097. https://doi.org/10.1175/JAS3465.1.

Pearson, K.J., Lister, G.M.S., Birch, C.E., Allan, R.P., Hogan, R.J. and Woolnough, S.J. (2014) Modelling the diurnal cycle of tropical convection across the 'grey zone'. *Quarterly Journal of the Royal Meteorological Society*, 140, 491–499.

Petrova, I.Y., Miralles, D.G., Van Heerwaarden, C.C. and Wouters, H. (2018) Relation between convective rainfall properties and antecedent soil moisture heterogeneity conditions in North Africa. *Remote Sensing*, 10, 969. https://doi.org/10.3390/rs10060969.

Rieck, M., Hohenegger, C. and van Heerwaarden, C.C. (2014) The influence of land surface heterogeneities on cloud size development. *Monthly Weather Review*, 142, 3830–3846. https://doi.org/10.1175/MWR-D-13-00354.1.

Rochetin, N., Couvreux, F. and Guichard, F. (2017a) Morphology of breeze circulations induced by surface flux heterogeneities and their impact on convection initiation. *Quarterly Journal of the Royal Meteorological Society*, 143, 463–478. https://doi.org/10.1002/qj.2935.

Sato, T., Miura, H., Satoh, M., Takayabu, Y.N. and Wang, Y. (2009) Diurnal cycle of precipitation in the tropics simulated in a global cloud-resolving model. *Journal of Climate*, 22, 4809–4826. https://doi.org/10.1175/2009JCLI2890.1.

Segal, M. and Arritt, R.W. (1992) Nonclassical mesoscale circulations caused by surface sensible heat-flux gradients. *Bulletin of the American Meteorological Society*, 73, 1593–1604. https://doi.org/10.1175/1520-0477.

Shipway, B.J. and Hill, A.A. (2012) Diagnosis of systematic differences between multiple parametrizations of warm rain microphysics using a kinematic framework. *Quarterly Journal of the Royal Meteorological Society*, 138, 2196–2211. https://doi.org/10.1002/qj.1913.

Shutts, G.J. and Gray, M.E.B. (1994) A numerical modelling study of the geostrophic adjustment process following deep convection. *Quarterly Journal of the Royal Meteorological Society*, 120, 1145–1178. https://doi.org/10.1002/qj.49712051903.

Stephens, G.L., L'Ecuyer, T., Forbes, R., Gettelmen, A., Golaz, J.-C., Bodas-Salcedo, A., Suzuki, K., Gabriel, P. and Haynes, J. (2010) Dreary state of precipitation in global models. *Journal of Geophysical Research: Atmospheres*, 115, D24211. https://doi.org/10.1029/2010JD014532.

Stirling, A.J. and Petch, J.C. (2004) The impacts of spatial variability on the development of convection. *Quarterly Journal of the Royal Meteorological Society*, 130, 3189–3206.

Stratton, R.A. and Stirling, A.J. (2012) Improving the diurnal cycle of convection in GCMs. *Quarterly Journal of the Royal Meteorological Society*, 138, 1121–1134.

Tan, J., Huffman, G.J., Bolvin, D.T. and Nelkin, E.J. (2019) Diurnal cycle of IMERG V06 precipitation. *Geophysical Research Letters*, 46, 13584–13592. https://doi.org/10.1029/2019GL085395.

Taylor, C.M., Gounou, A., Guichard, F., Harris, P.P., Ellis, R.J., Couvreux, F. and De Kauwe, M. (2011) Frequency of Sahelian storm initiation enhanced over mesoscale soil-moisture patterns. *Nature Geoscience*, 4, 430.

Taylor, C.M., Parker, D.J. and Harris, P.P. (2007) An observational case study of mesoscale atmospheric circulations induced by soil moisture. *Geophysical Research Letters*, 34, L15801. https://doi.org/10.1029/2007GL030572.

Volonté, A., Clark, P.A. and Gray, S.L. (2020) Idealised simulations of cyclones with robust symmetrically unstable sting jets. *Weather and Climate Dynamics*, 1, 63–91. https://doi.org/10.5194/wcd-1-63-2020.

Walters, D., Baran, A.J., Boutle, I., Brooks, M., Earnshaw, P., Edwards, J., Furtado, K., Hill, P., Lock, A., Manners, J., Morcrette, C., Mulcahy, J., Sanchez, C., Smith, C., Stratton, R., Tennant, W., Tomassini, L., Van Weverberg, K., Vosper, S., Willett, M., Browse, J., Bushell, A., Carslaw, K., Dalvi, M., Essery, R., Gedney, N., Hardiman, S., Johnson, B., Johnson, C., Jones, A., Jones, C., Mann, G., Milton, S., Rumbold, H., Sellar, A., Ujiie, M., Whitall, M., Williams, K. and Zerroukat, M. (2019) The Met Office Unified Model Global Atmosphere 7.0/7.1 and JULES Global Land 7.0 configurations. *Geoscientific Model Development*, 12, 1909–1963. https://doi.org/10.5194/gmd-12-1909-2019.

Willett, M. R. and Whitall, M. A. (2017) *A simple prognostic based convective entrainment rate for the Unified model: description and tests*. Forecasting Research Technical Report. Available at: https://library.metoffice.gov.uk/Portal/Default/en-GB/RecordView/Index/%633651.

Wilson, D.R. and Ballard, S.P. (1999) A microphysically based precipitation scheme for the UK Meteorological Office Unified Model. *Quarterly Journal of the Royal Meteorological Society*, 125, 1607–1636. https://doi.org/10.1002/qj.49712555707.

Wilson, D.R., Bushell, A.C., Kerr-Munslow, A.M., Price, J.D. and Morcrette, C.J. (2008) PC2: a prognostic cloud fraction and condensation scheme. I: Scheme description. *Quarterly Journal of the Royal Meteorological Society*, 134, 2093–2107. https://doi.org/10.1002/qj.333.

Wing, A.A., Stauffer, C.L., Becker, T., Reed, K.A., Ahn, M.-S., Arnold, N.P., Bony, S., Branson, M., Bryan, G.H., Chaboureau, J.-P., de Roode, S.R., Gayatri, K., Hohenegger, C., Hu, I.-K., Jansson, F., Jones, T.R., Khairoutdinov, M., Kim, D., Martin, Z.K., Matsugishi, S., Medeiros, B., Miura, H., Moon, Y., Müller, S.K., Ohno, T., Popp, M., Prabhakaran, T., Randall, D., Rios-Berrios, R., Rochetin, N., Roehrig, R., Romps, D.M., Ruppert, J.H., Jr., Satoh, M., Silvers, L.G., Singh, M.S., Stevens, B., Tomassini, L., van Heerwaarden, C.C., Wang, S. and Zhao, M. (2020) Clouds and convective self-aggregation in a multimodel ensemble of radiative-convective equilibrium simulations. *Journal of Advances in Modeling Earth Systems*, 12, e2020MS002138. https://doi.org/10.1029/2020MS002138.

Wood, N., Staniforth, A., White, A., Allen, T., Diamantakis, M., Gross, M., Melvin, T., Smith, C., Vosper, S., Zerroukat, M. and Thuburn, J. (2014) An inherently mass-conserving semi-implicit semi-Lagrangian discretization of the deep-atmosphere global non-hydrostatic equations. *Quarterly Journal of the Royal Meteorological Society*, 140, 1505–1520. https://doi.org/10.1002/qj.2235.

Wu, C.-M., Lo, M.-H., Chen, W.-T. and Lu, C.-T. (2015) The impacts of heterogeneous land surface fluxes on the diurnal cycle precipitation: a framework for improving the GCM representation of land-atmosphere interactions. *Journal of Geophysical Research: Atmospheres*, 120, 3714–3727.

Xiao, H., Berg, L.K. and Huang, M. (2018) The impact of surface heterogeneities and land-atmosphere interactions on shallow clouds over ARM SGP site. *Journal of Advances in Modeling Earth Systems*, 10, 1220–1244. https://doi.org/10.1029/2018MS001286.

Xie, S., Wang, Y.-C., Lin, W., Ma, H.-Y., Tang, Q., Tang, S., Zheng, X., Golaz, J.-C., Zhang, G.J. and Zhang, M. (2019) Improved diurnal cycle of precipitation in E3SM with a revised convective triggering function. *Journal of Advances in Modeling Earth Systems*, 11, 2290–2310. https://doi.org/10.1029/2019MS001702.

Yang, G.-Y. and Slingo, J. (2001) The diurnal cycle in the tropics. *Monthly Weather Review*, 129, 784–801.

Young, G., Connolly, P.J., Jones, H.M. and Choularton, T.W. (2017) Microphysical sensitivity of coupled springtime Arctic stratocumulus to modelled primary ice over the ice pack, marginal ice, and ocean. *Atmospheric Chemistry and Physics*, 17, 4209–4227. https://doi.org/10.5194/acp-17-4209-2017.

How to cite this article: Harvey, N.J., Daleu, C.L., Stratton, R.A., Plant, R.S., Woolnough, S.J. & Stirling, A.J. (2022) The impact of surface heterogeneity on the diurnal cycle of deep convection. *Quarterly Journal of the Royal Meteorological Society*, 148(749), 3509–3527. Available from: https://doi.org/10.1002/qj.4371